Submitted to the Annals of Applied Statistics
arXiv: arXiv:0000.0000

A BAYESIAN FUNCTIONAL LINEAR COX REGRESSION MODEL (BFLCRM) FOR PREDICTING TIME TO CONVERSION TO ALZHEIMER'S DISEASE*

By Eunjee Lee[†], Hongtu Zhu[†], Dehan Kong[†], Yalin Wang[‡], Kelly Sullivan Giovanello[†], Joseph G Ibrahim[†] and for the Alzheimer's Disease Neuroimaging Initiative

University of North Carolina at Chapel Hill[†] and Arizona State University[‡]

The aim of this paper is to develop a Bayesian functional linear Cox regression model (BFLCRM) with both functional and scalar covariates. This new development is motivated by establishing the likelihood of conversion to Alzheimer's disease (AD) in 346 patients with mild cognitive impairment (MCI) enrolled in the Alzheimer's Disease Neuroimaging Initiative 1 (ADNI1) and the optimal early markers of conversion. These 346 MCI patients were followed over 48 months, with 161 MCI participants progressing to AD at 48 months. The functional linear Cox regression model was used to establish that functional covariates including hippocampus surface morphology and scalar covariates including brain MRI volumes, cognitive performance (ADAS-Cog), and APOE status can accurately predict the conversion time to AD. Posterior computation proceeds via an efficient Markov chain Monte Carlo algorithm. A simulation study is performed to evaluate the finite sample performance of BFLCRM.

1. Introduction. Alzheimer's Disease (AD) is a firmly incurable and progressive disease [10]. In the pathology of AD, mild cognitive impairment (MCI) is a clinical syndrome characterized by insidious onset and gradual progression, and commonly arising as a result of underlying neurodegenerative pathology [19]. Since MCI is considered as a risk state for AD, a major

* Address for correspondence and reprints: Hongtu Zhu, Ph.D., Email: hzhu@bios.unc.edu. The research of Drs. Zhu and Ibrahim was supported by NIH grants RR025747-01, GM70335, CA74015, P01CA142538-01, MH086633, EB005149-01 and AG033387. The content is solely the responsibility of the authors and does not necessarily represent the official views of the NIH. Data used in preparation of this article were obtained from the Alzheimer's Disease Neuroimaging Initiative (ADNI) database (adni.loni.usc.edu). As such, the investigators within the ADNI contributed to the design and implementation of ADNI and/or provided data but did not participate in analysis or writing of this report. A complete listing of ADNI investigators can be found at: http://adni.loni.usc.edu/wpcontent/uploads/how_to_apply/ADNI_Acknowledgement_List.pdf.

MSC 2010 subject classifications: Primary 60K35, 60K35; secondary 60K35

Keywords and phrases: Alzheimer's disease, hippocampus surface morphology, mild cognitive impairment, proportional hazard model

research focus in recent years has been to delineate a set of biomarkers that provide evidence of such a neurodegenerative pathology in living individuals, with the goal of specifying the likelihood that the pathophysiological process is due to Alzheimer's disease (MCI due to AD; MCI-AD) and will lead to dementia within a few years [1]. Accordingly, increasing attention has been devoted to investigate the utility of various imaging, genetic, clinical, behavioral, and fluid data to predict the conversion from MCI to AD.

Several studies have utilized a small subset of biosignatures and then assessed the relative importance of different modalities in predicting the diagnostic change from MCI to AD [9, 15, 46, 49, 61]. For example, in [9], the authors simultaneously examined multiple features from different modalities of data, including structural magnetic resonance imaging (MRI) morphometry, cerebrospinal fluid biomarkers, and neuropsychological measures to assess an optimal set of predictors of conversion from MCI to AD. They observed that structural changes within the medial temporal lobe (MTL), particularly the hippocampus, as well as performance on cognitive tests that rely on MTL integrity (i.e., episodic memory), were good predictors of MCI to AD conversion.

Recently, most researchers have turned to the analysis of longitudinal data to assess the dynamic changes of various biomarkers associated with the MCI-to-AD transition across time. To begin, a prominent neural correlate of MCI-AD is volume loss within the MTL, especially within the hippocampus and entorhinal cortex [13], with increasing atrophy in these structures from normal aging to MCI to AD [42]. Longitudinal studies of individuals with MCI-AD have also highlighted the importance of assessing MTL changes in tracking the progression of MCI to AD. For example, several studies have documented diminished baseline hippocampal and entorhinal volumes that are associated with an increased likelihood of progressing to clinical dementia [21, 32]. Additionally, several modalities of disease indicators have been studied to assess progression to AD, including neuroimaging biomarkers [49, 57, 60]; biomedical biomarkers [51], and neuropsychological assessments [43]. Finally, a number of structural MRI studies, covering the region of interest (ROI), volume of interest, voxel-based morphometry, and shape analysis have reported that the degree of atrophy in several brain regions, such as the hippocampus and entorhinal cortex, is not only sensitive to disease progression, but predicts MCI conversion [7, 11, 38].

Despite the importance of these investigations, a central question remains. Namely, how do we accurately predict the time to conversion in individuals who harbor AD pathology, as well as determine the optimal early markers of conversion? In [55], 148 MCI subjects were used to identify the most predic-

tive neuropsychological measures. In [34], 139 MCI subjects in ADNI1 were used to evaluate the predictive power of brain volume, ventricular volume, hippocampus volume, APOE status, cerebrospinal fluid (CSF) biomarkers, and behavioral scores. Their results show a moderately accurate prediction with the value of an area under the curve of 0.757 at 36 months, whereas they found that baseline volumetric MRI and behavioral scores were selectively predictive. Finally, in 381 MCI subjects from ADNI 1 were examined to evaluate several biomarkers for predicting MCI to AD conversion including spatial patterns of brain atrophy, ADAS-Cog, APOE genotype, and cerebrospinal fluid (CSF) biomarkers. Their findings suggest that a combination of spatial patterns of brain atrophy and ADAS-Cog offers a good predictive power of conversion from MCI to AD, whereas APOE genotype did not significantly improve prediction. To the best of our knowledge, no prior study has examined the role of functional covariates including hippocampus surface morphology in predicting time to conversion from MCI to AD with/without adjusting for low-dimensional behavioral and clinical measures.

To assess the predictability of hippocampus surface morphology in survival models, we develop a Bayesian functional linear Cox regression model (BFLCRM) with both functional and scalar covariates. The BFLCRM integrates a Cox proportional-hazard regression and functional linear model into a single framework. First, BFLCRM can be an important extension of various statistical models including parametric, semiparametric and nonparametric models for handling survival response data and scalar covariates. See overviews of various survival models in [18, 24, 31] and the references therein. Recent advances in computation and prior elicitation have made Bayesian analysis of these survival models with scalar covariates feasible. For instance, nonparametric prior processes including the gamma process prior, the Beta process model, the correlated gamma process, and the Dirichlet process prior have been developed as the prior distribution of the baseline cumulative hazard function [24, 54]. Second, the BFLCRM can be an important extension of various functional linear models for handling discrete or continuous response data and functional covariates. The existing literature focuses on the development of frequentist methods for functional linear models. Some examples include [17, 28, 47, 48, 59] and the references therein. Third, the BFLCRM can be regarded as an important extension of high-dimensional survival models. However, most high-dimensional survival models focus on the identification of a small set of covariates and their overall effect on time-to-event outcomes [4, 29, 33]. These approaches can be suboptimal for high-dimensional imaging data, since the effect of imaging data

on clinical data and other imaging data is often *non-sparse*, which makes it notoriously difficult for many existing regularization methods [14, 56].

In Section 2, we will introduce BFLCRM and its associated Bayesian estimation procedure. In Section 3, we will introduce the NIH Alzheimer's Disease Neuroimaging Initiative (ADNI) dataset and illustrate the use of BFLCRM in the prediction of time to conversion from MCI to AD by using both functional and scalar covariates. In Section 4, we conduct simulation studies to examine the finite sample performance of BFLCRM. Section 5 presents concluding remarks.

2. Bayesian Functional Linear Cox Regression Models.

2.1. *Model Setup.* Consider imaging, genetic, and clinical data from $n = 346$ independent MCI patients in ADNI1. For the i-th MCI patient, we observe a possibly right censored time to conversion to AD, denoted by y_i. Specifically, $y_i = T_i \wedge C_i$ is the minimum of the censoring time C_i and the transition time T_i and $\nu_i = \mathbf{1}(y_i = T_i)$, where $\mathbf{1}(\cdot)$ is an indicator function. Moreover, we also observe a $p \times 1$ vector of scalar covariates, denoted by $\mathbf{x}_i = (x_{i1}, \cdots, x_{ip})^T$, and a functional covariate, denoted by $Z_i(\cdot)$, measured at a set of grid points in a compact set, denoted by $\mathcal{S}$. The scalar covariates of interest include age at baseline, length of eduction, gender, handedness, marital status, retirement, and the well-known Apolipoprotein E (APOE) SNPs. ApoE is polymorphic with three major isoforms: ApoE2 (cys112, cys158), ApoE3 (cys112, arg158), and ApoE4 (arg112, arg158). The functional covariate of interest is the hippocampus surface morphology.

Our problems of interest are to establish the likelihood of conversion to Alzheimer's disease (AD) in 373 MCI patients enrolled in the ADNI1 and to select the optimal early markers of conversion from both the scalar covariates and the functional covariate. With the sole presence of $\mathbf{x}_i$, it is common to consider Cox's proportional hazards model [8], which assumes that the conditional hazard function of y_i given $\mathbf{x}_i$ is given by

$$h(y|\mathbf{x}_i) = h_0(y)\exp(\mathbf{x}_i^T\boldsymbol{\beta}) = h_0(y)\exp(\sum_{k=1}^{p} x_{ik}\beta_k), \tag{2.1}$$

where $\boldsymbol{\beta} = (\beta_1, \cdots, \beta_p)^T$ is a $p \times 1$ vector of regression coefficients and $h_0(\cdot)$ is an unknown baseline hazard function. However, the Cox proportional hazards model (2.1) does not incorporate the effect of the functional covariate $Z_i(\cdot)$ on the time to conversion.

We propose a functional linear Cox regression model with three components for handling both functional and scalar covariates as a natural extension of (2.1). In the first component of FLCRM, it is assumed that the

hazard function of y_i given $(\mathbf{x}_i, Z_i(\cdot))$ is given by

$$h(y|\mathbf{x}_i, Z_i(\cdot)) = h_0(y)\exp(\sum_{k=1}^{p} x_{ik}\beta_k + \int_{\mathcal{S}} \gamma(s)Z_i(s)ds), \tag{2.2}$$

where $\gamma(\cdot)$ is an unknown coefficient function in S.

The second component of FLCRM is the functional principal component analysis (fPCA) model of $Z_i(\cdot)$'s. It is assumed that the $Z_i(s)$'s are given by

$$Z_i(s) = \tilde{Z}_i(s) + \epsilon_i(s) = \mu(s) + \sum_{j=1}^{\infty} \xi_{ij}\phi_j(s) + \epsilon_i(s), \tag{2.3}$$

where $\mu(s)$ is the mean function of $Z_i(s)$ (or $\tilde{Z}_i(s)$), $\xi_{ij} = \int_{\mathcal{S}}(Z_i(s) - \mu(s))\phi_j(s)ds$'s are functional principal component (fPC) scores, and the $\epsilon_i(s)$'s are measurement errors with mean zero and variance $\sigma^2_\epsilon(s)$ at each s and independent of each other for $s \neq s'$. Moreover, we consider the covariance function of $\{\tilde{Z}_i(s) : s \in S\}$, denoted by $K(s,s') = E\{(\tilde{Z}(s) - \mu(s))(\tilde{Z}(s') - \mu(s'))\}$ and assume that $K(s,s')$ admits a spectral decomposition $K(s,s') = \sum_{j=1}^{\infty} \psi_j\phi_j(s)\phi_j(s')$, where $(\psi_j, \phi_j(s))$'s are the eigenvalue-eigenfunction pairs of $K(s,s')$. Thus, $\tilde{Z}_i(s) - \mu(s)$ admits the Karhunen-Loeve expansion of $\tilde{Z}_i(s) - \mu(s) = \sum_{j=1}^{\infty} \xi_{ij}\phi_j(s)$. For each fixed j, the ξ_{ij}s are uncorrelated random variables with mean zero and variance ψ_j.

The third component of the FLCRM is an approximation of $\int_{\mathcal{S}} \boldsymbol{\gamma}(s)Z_i(s)ds$. Since the eigenfunctions $\psi_j(\cdot)$ form an orthonormal system on the space of square-integrable functions on $\mathcal{S}$, the covariate function $\gamma(s)$ is assumed to be expanded as

$$\gamma(s) = \sum_{j=1}^{\infty} \phi_j(s)\gamma_j \quad \text{with} \quad \sum_{j=1}^{\infty} \gamma_j^2 < \infty. \tag{2.4}$$

Therefore, we have

$$\int_{\mathcal{S}} Z_i(s)\gamma(s)ds = \int_{\mathcal{S}} \mu(s)\gamma(s)ds + \sum_{j=1}^{\infty} \xi_{ij}\gamma_j. \tag{2.5}$$

By introducing a new baseline hazard function $h_0'(s) = h_0(s)\exp\left(\int \mu(s)\gamma(s)ds\right),$, we can approximate $h(y|\mathbf{x}_i, Z_i(\cdot))$ as

(2.6)

$$h_0'(y)\exp\left(\sum_{k=1}^{p} x_{ik}\beta_k + \sum_{j=1}^{\infty} \xi_{ij}\gamma_j\right) \approx h_0'(y)\exp\left(\sum_{k=1}^{p} x_{ik}\beta_k + \sum_{j=1}^{q_n} \xi_{ij}\gamma_j\right),$$

where q_n is a sufficiently large integer that may depend on n. As shown in the literature, such an approximation is accurate under some conditions on the decay rate of the γ_j's. Practically, it is common to choose q_n such that the percentage of variance explained by the first q_n fPCA components is 70%, 85%, or 95%. Alternatively, we may formulate it as a model selection procedure and choose it by using some model selection criterion, such as the deviance information criterion (DIC) [26].

2.2. *Priors.* To carry out a Bayesian analysis of model (2.5), we specify a joint priors for all unknown parameters $(\boldsymbol{\beta}, \boldsymbol{\gamma}, H_0)$, where $H_0(\cdot)$ is the cumulative hazard function of $h_0'(\cdot)$. We first set $p(\boldsymbol{\beta}, \boldsymbol{\gamma}, H_0) = p(\boldsymbol{\beta}, \boldsymbol{\gamma})p(H_0)$ and assume $(\boldsymbol{\beta}, \boldsymbol{\gamma}) \sim N(\boldsymbol{\mu}_0, \Sigma_0)$, where $N(\boldsymbol{\mu}_0, \Sigma_0)$ is the multivariate normal distribution with $(p + q_n) \times 1$ mean vector $\boldsymbol{\mu}_0$ and a $(p + q_n) \times (p + q_n)$ covariance matrix Σ_0. If $\lambda_{min}(\Sigma_0)$ converges to ∞, then $N(\mu_0, \Sigma_0)$ tends to be an improper prior. In contrast, if $\lambda_{max}(\Sigma_0)$ is very small, then $N(\mu_0, \Sigma_0)$ tends to be a strongly informative prior.

We may specify different prior distributions for $H_0(y)$. The most convenient and popular distribution for $H_0(y)$ is the piecewise constant hazard model. Specifically, we first construct a finite partition of the time axis, $0 < s_1 < s_2 < \ldots < s_J$, with $s_J > y_i$ for all i, which leads to J intervals $(0, s_1]$, ..., $(s_{J-1}, s_J]$. In the $j-$th interval, we set $h_0(y) = \lambda_j$ for $y \in I_j = (s_{j-1}, s_j]$. A common prior of the baseline hazard $\boldsymbol{\lambda} = (\lambda_1, \cdots, \lambda_J)^T$ is the independent gamma prior $\lambda_j \sim \mathcal{G}(\alpha_{0j}, \alpha_{1j})$ for $j = 1, \ldots, J$, where α_{0j} and α_{1j} are prior hyperparameters. Another approach is to build prior correlation among the λ_j's using a prior $\boldsymbol{\psi} \sim N(\boldsymbol{\psi}_0, \Sigma_J)$, where $\psi_j = \log(\lambda_j)$ for $j = 1, \ldots, J$ and $\psi_j = (\psi_1, \cdots, \psi_J)$.

We may consider a gamma process prior for $H_0(y)$, that is, $H_0 \sim \mathcal{G}P(c_0 H^*, c_0)$ [30], where c_0 is a fixed scalar and $H^*(y) = \int_0^y h_0'(t)dt$ is an known increasing function with $H^*(0) = 0$. That is, $H^*(y)$ is the mean of the process and $\{H_0(y) : y \geq 0\}$ is a stochastic process with the properties: $H_0(0) = 0$; $H_0(z)$ has independent increments in disjoint intervals; and for $t > s$, $H_0(t) - H_0(s) \sim \mathcal{GP}(c_0(H^*(t) - H^*(s)), c_0)$. For notational simplicity, we focus on the piecewise constant hazard model from here on.

2.3. *Posterior Computation.* The log-posterior distribution of $(\boldsymbol{\beta}, \boldsymbol{\gamma}, H_0)$ (unnormalized) is given by

$$\begin{aligned}&\sum_{i=1}^{n}\sum_{j=1}^{J}[u_{ij}\nu_i(\log\lambda_j + \boldsymbol{z}_i^T\boldsymbol{\theta}) - u_{ij}\{\lambda_j(y_i - s_{j-1}) + \sum_{g=1}^{j-1}\lambda_g(s_g - s_{g-1})\}\exp(\boldsymbol{z}_i^T\boldsymbol{\theta})]\\ &+\{\log|\boldsymbol{\Sigma}_0| + (\boldsymbol{\theta}-\boldsymbol{\mu}_0)^T\Sigma_0^{-1}(\boldsymbol{\theta}-\boldsymbol{\mu}_0)\}/2\\ &\qquad + \sum_{j=1}^{J}\{(\alpha_{0j}-1)\log\lambda_j - \lambda_j\alpha_{1j} + \alpha_{0j}\log(\alpha_{1j}) - \log\Gamma(\alpha_{0j})\},\end{aligned} \tag{2.7}$$

where $\boldsymbol{\theta} = (\boldsymbol{\beta}^T, \boldsymbol{\gamma}^T)^T$, $\boldsymbol{z}_i = (\boldsymbol{x}_i^T, \xi_{i1}, \cdots, \xi_{iq_n})^T$, and $s_0 = 0$. Moreover, $u_{ij} = 1$ if the $i-$th subject is right censored in the $j-$th interval and 0 otherwise. We propose a Gibbs sampler for posterior computation after truncating the sum of the infinite series to have $q_n < \infty$ terms. The Gibbs sampler is computationally efficient and mixes rapidly. We first specify the hyperparameters $\boldsymbol{\mu}_0, \Sigma_0, \alpha_{0j}$ and α_{1j} for all j at appropriate values. Starting from the initiation step, the Gibbs sampler for model (2.6) with the truncated term q_n proceeds as follows:

1. Update $(\boldsymbol{\beta}, \boldsymbol{\gamma})$ according to their full conditional distribution in (2.7). Specifically, we employ the random walk Metropolis-Hastings (M-H) [22, 37] and choose a normal proposal density yielding an average acceptance rate of 23.4% [20].
2. Update λ_j from its full conditional distribution

$$p(\lambda_j|\boldsymbol{\lambda}_0^{(-j)}, -) \sim \text{Gamma}(\alpha_{0j} + \sum_{i=1}^{n} u_{ij}\nu_i, \tilde{\alpha}_{1j}),$$

where $\boldsymbol{\lambda}_0^{(-j)}$ is the $\boldsymbol{\lambda}_0$ vector without the j-th element and $\tilde{\alpha}_{1j}$ is given by

$$\tilde{\alpha}_{1j} = \begin{cases} \alpha_{1j} + \sum_{i=1}^{n}\{u_{ij}(y_i - s_{j-1}) + (s_j - s_{j-1})\sum_{k=j+1}^{J} u_{ik}\}\exp(\boldsymbol{z}_i^T\boldsymbol{\theta}), \\ \qquad\qquad \text{if } j \le J-1; \\ \alpha_{1J} + \sum_{i=1}^{n}\{u_{iJ}(y_i - s_{J-1})\exp(\boldsymbol{z}_i^T\boldsymbol{\theta})\}, \\ \qquad\qquad \text{if } j = J. \end{cases}$$

3. Alzheimer's Disease Neuroimaging Initiative Data Analysis.

3.1. *Alzheimer's Disease Neuroimaging Initiative.* The development of the BFLCRM is motivated by the analysis of imaging, genetic, and clinical data collected by ADNI. Data used in the preparation of this article

were obtained from the Alzheimer's Disease Neuroimaging Initiative (ADNI) database (adni.loni.usc.edu). ADNI is a global study that supports investigation of treatment to intervene the progression of Alzheimers Disease (AD). Detection of very early AD progression will lead researchers and clinicians to develop new treatments and conduct clinical trials efficiently. The ADNI study has aimed to detect and monitor the early stage of Alzheimers Disease (AD) by investigating serial magnetic resonance imaging (MRI), positron emission tomography (PET), genetic, and biochemical biomarkers, and neuropsychological and clinical assessment. The Principal Investigator of this initiative is Michael W. Weiner, MD, VA Medical Center and University of California, San Francisco. The ADNI began in 2004 and recruited 400 subjects with mild cognitive impairment (MCI), 200 subjects with early AD and 200 cognitively normal elderly from over 50 sites across the U.S. and Canada. This multicite, longitudinal study was financially supported as $67 million by National Institute on Aging (NIA), the National Institute of Biomedical Imaging and Bioengineering (NIBIB), the Food and Drug Administration (FDA), and 13 private pharmaceutical companies. This initial phase is called ADNI1, which was extended with ADNI GO in 2009. ADNI GO investigated the existing ADNI1 cohort and included 200 participants diagnosed as having early MCI (EMCI). In 2011, ADNI2 began to study participants from the ADNI1/ADNI GO and added 150 elderly controls, 100 EMCI participants, 150 late MCI (LMCI) participants and 150 MCI patients. For up-to-date information, see www.adni-info.org.

3.2. *Data Description.* The aim of this ADNI data analysis is to examine the predictability of clinical, genetic, and imaging data for the time to conversion to AD in MCI patients. We focused on 346 MCI patients at baseline of the ADNI1 database. Among the 346 MCI patients, 151 of them are converters and 195 are non-converters at 48 months.

For each MCI patient, we included his/her clinical, genetic, and imaging variables at baseline. The clinical characteristics include Gender (1=Male; 2=Female), Handedness (1=Right; 2=Left), Marital Status (1=Married; 2=Widowed; 3=Divorced; 4=Never married), Education length, Retirement (1=Yes; 0=No), Age, and Alzheimer's Disease Assessment Scale-Cognition (ADAS-Cog) score. The ADAS-Cog test has been widely used to assess the severity of dysfunction in adults [50]. The genetic variables include the APOE genetic covariates, since it is well known that mutations in APOE raise the risk of progression from amnestic MCI to AD[44]. The Apolipoprotein E (APOE) SNPs, rs429358 and rs7412 were genotyped separately in ADNI1. These two SNPs together define a 3 allele haplotype, namely the

$\epsilon 2$, $\epsilon 3$, and $\epsilon 4$ variants and the presence of each of these variants was available in the ADNI database for all the individuals. In addition, we selected 7 regions of interest (ROIs) which may significantly influence MCI progression among the 93 ROI volume data [5, 16, 27]. These 7 ROIs are bilateral hippocampal formation, bilateral amygdala, posterior limb of internal capsule, bilateral thalamus. In total, we have 19 scalar covariates. The imaging data include the hippocampal radial distances of 30,000 surface points on the left and right hippocampal surfaces. The hippocampal radial distance is a distance from its medial core to the hippocampal surface and measures hippocampal thickness.

In the demographic information, 220 participants are male, and 126 are female; 316 are right-handed, and 30 are left-handed. For Marital Status, 283 were married, 40 were widowed, 19 were divorced, and 4 were never married at baseline. Among these individuals, 276 were retired and 70 were not. On average, the subjects had 15.7 years of education with standard deviation 3.0 years, the minimum 6 years, and the maximum 20 years. The average age of subjects was 75.0 years with standard deviation of 7.3 years. The youngest person was 55 years old, while the oldest person was 90 years old. For the genetics information on the first allele of APOE4, 25 subjects had genotype 2, 277 had genotype 3, and 44 had genotype 4. For the second allele, 156 had genotype 3, while 190 had genotype 4. The average ADAS-cog score was 11.5, with standard deviation of 4.4. The lowest score was 2 and the highest score was 27.67.

3.3. *Hippocampus Image Preprocessing.* In imaging processing steps for the hippocampal surface data, we adopted a surface fluid registration based hippocampal subregional analysis package [52]. I uses isothermal coodinates and fluid registration to generate one-to-one hippocampal surface registration for following surface statistics computation. This software package has been adopted by various studies [6, 36, 39, 53]. Given the 3D MRI scans, hippocampal substructures were segmented with FIRST [41] and hippocampal surfaces were automatically reconstructed with the marching cube method [35]. We applied an automatic algorithm, topology optimization, to introduce two cuts on a hippocampal surface to convert it into a genus zero surface with two open boundaries. The locations of the two cuts were at the front and back of the hippocampal surface, representing its anterior junction with the amygdala, and its posterior limit as it turns into the white matter of the fornix. Then holomorphic 1-form basis functions were computed [58]. These induced conformal grids the hippocampal surfaces which wereare consistent across subjects. With this conformal grid, we computed the conformal rep-

resentation of the surface [52], i.e., the conformal factor and mean curvature, which represent the intrinsic and extrinsic features of the surface, respectively. The "feature image" of a surface was computed by combining the conformal factor and mean curvature and linearly scaling the dynamic range into [0, 255]. Next, we registered the feature image of each surface in the dataset to a common template with an inverse consistent fluid registration algorithm. With conformal parameterization, we essentially converted a 3D surface registration problem into a 2D image registration problem. The flow induced in the parameter domain establishes high-order correspondences between 3D surfaces. Finally, various surface statistics were computed on the registered surface, such as multivariate tensor-based morphometry (mTBM) statistics [58], which retain the full tensor information of the deformation Jacobian matrix, together with the radial distance [45], which retains information on the deformation along the surface normal direction.

3.4. *Data Analysis.* We focused on 346 MCI patients in the ADNI1 data in order to examine the predictability of clinical, genetic, and imaging covariates for the time to conversion to AD from MCI. The patients consist of 151 converters and 195 non-converters. We fit the BFLCRM with time to conversion to AD as the response y_i, the clinical and genetic data as scalar covariates in $\boldsymbol{x}_i$, and the hippocampus surface data as functional covariates in $Z_i(\cdot)$. To estimate ξ_{ij}, we employed the local linear regression technique to estimate all the $\tilde{Z}_i(s)$'s and then used their sample and covariance functions to estimate $\mu(s)$ and $K(s, s')$. Subsequently, we estimated $\phi_i(s)$ and ξ_{ij} for all the $i, j \leq n$. For the piecewise constant hazards model of $H_0(\cdot)$, we chose $J = 13$ intervals so that each interval contains at least one failure or censored observation. We set the MLE for regression coefficients of a piecewise constant hazards model as $\boldsymbol{\mu}_0$, $diag(0.1^2, \cdots, 0.1^2)$ as Σ_0, and $\alpha_{0j} = 8, \alpha_{1j} = 10$, for $j = 1, \cdots, 13$. We ran the Gibbs sampler for 25,000 iterations after 5,000 burn-in iterations for each fixed $q_n = 12$.

We chose the first 12 eigenfunctions of hippocampal surface data, which explain about 71.20% of the variance in the hippocampus surface data. The final BFLCRM model (2.6) contains 19 scalar covariates and the first 12 fPC scores. Based on the 20,000 MCMC samples, we calculated various posterior quantities of $(\boldsymbol{\beta}, \boldsymbol{\gamma}, \boldsymbol{\lambda})$. Table 1 shows the posterior means of the regression coefficients $\boldsymbol{\beta}$ and their standard deviations, as well as the lower and upper limits of the 95% highest posterior density (HPD) intervals. The 95% HPD interval for a scalar parameter is the interval such that 95% of the highest area of the posterior density is contained in this interval[25]. Seven scalar covariates including "Gender", "Handedness", "first allele in APOE4=3",

"the first allele in APOE4=4, " "Second allele in APOE4=3", and "ADAS-cog score" have HPD intervals that do not contain 0.

Moreover, the 1st, 7th, 9th and 11th fPCs have 95% HPD intervals that do not contain 0. This may indicate that the hippocampal radial distance is an important functional covariate to predict the time to conversion to AD in MCI subjects. Furthermore, we estimated the coefficient function $\gamma(\cdot)$ by using $\hat{\gamma}(s) = \sum_{j=1}^{12} \hat{\phi}_j(s)\hat{\gamma}_j$, where $\hat{\gamma}_j$ was the posterior mean of γ_j for each j. Figure 1 shows the estimated coefficient function $\hat{\gamma}(\cdot)$ associated with the hippocampal surface data. The color bar in the Figure 1 contains 12 different colors, and there are 11 lines between these bars. From low to high, the 11 values are 11 equally spaced between [-0.0037, 0.0059], where the starting point and ending point are the left and right end of the interval. A red region suggests that the thinner the area is on the hippocampus, the shorter the time to conversion to AD is. A blue region suggests that the thicker the area is on the hippocampus, the shorter the time to conversion to AD is. Inspecting Figure 1 reveals that the subfields of CA1, CA2, CA3, and subicular on the hippocampus have positive effects on the hazard function, indicating that the thinner these areas are on the hippocampus, the shorter the time to conversion to AD is.

We plotted the survival functions for male and female patients, where the values of other covariates are taken as the mean value of the covariates. Also the average patient whose the first/second allele in APOE4 is 3/4 or not, where the values of other covariates are taken as the mean value of the covariates. Also the average patient who have never married or not, where the values of other covariates are taken as the mean value of the covariates; see Figure 2. It is noticed that the average female subjects tend to convert from MCI to AD more fastly than the average male subjects. The subjects who have type 2 of the first allele in APOE4 tend to convert from MCI to AD more fastly than the other subjects. The subjects with type 4 of the first allele in APOE4 are expected to convert from MCI to AD more fastly than the other subjects. The subjects who have married are more hazardous than the other subjects.

Finally, we compared the full model discussed above to several reduced models in order to compare their predictive performance. We considered three additional models. Model 1 includes all the covariates except the ROI volume covariates. Model 2 includes all the covariates except the hippocampus surface data. Model 3 includes only the clinical covariates, APOE4, and the ADAS-cog score. We calculated the DIC and integrated AUC (iAUC) for all four models, where AUC denotes the area under the Receiver Operating Characteristic (ROC) curve.

For all the reduced models, We set $J = 13$ intervals so that each interval contains at least one failure or censored observation. The MLE for regression coefficients of a piecewise constant hazards model was chosen to be $\boldsymbol{\mu}_0$. We let $diag(0.1^2, \cdots, 0.1^2)$ as Σ_0, and $\alpha_{0j} = 8, \alpha_{1j} = 10$, for $j = 1, \cdots, 13$. We ran the Gibbs sampler for 25,000 iterations after 5,000 burn-in iterations.

For Model 1, we excluded the ROI volume covariates from the the full model. We applied BFLCRM to obtain the estimation results for the 24 covariates. Based on the 20,000 MCMC samples, "Gender", "Handedness", "Never married", "Retirement","first allele in APOE4=3", "the first allele in APOE4=4, " "Second allele in APOE4=3", and "ADAS-cog score" have HPD intervals that do not contain 0. The 1st, 3rd, 7th, 9th and 11th fPCs have 95% HPD intervals that do not contain 0. Inspecting Figure 3 reveals that the subfields of CA1, CA2, CA3, and subicular on the hippocampus have positive effects on the hazard function, indicating that the thinner these areas are on the hippocampus, the shorter the time to conversion to AD is. Compared with the full model results, the red areas are broader for Model 1. We plotted the survival functions for male and female patients, where the values of other covariates are taken as the mean value of the covariates. The average patient whose the first/second allele in APOE4 is 3/4 or not, where the values of other covariates are taken as the mean value of the covariates. Also the average patient who have never married or not, where the values of other covariates are taken as the mean value of the covariates; see Figure 4. It is noticed that the average female subjects tend to convert from MCI to AD more fastly than the average male subjects. The subjects who have type 2 of the first allele in APOE4 tend to convert from MCI to AD more fastly than the other subjects. The subjects with type 3 of the first allele in APOE4 are expected to convert from MCI to AD more fastly than the other subjects. The subjects who have married are more hazardous than the other subjects.

For Model 2, we excluded the hippocampal surfaces covariates from the the full model. We applied BFLCRM to obtain the estimation results for the 19 covariates. Based on the 20,000 MCMC samples, "Gender", "Handedness", "Age", "Never married", "Retirement", "first allele in APOE4=3", "the first allele in APOE4=4, " "Second allele in APOE4=3", and "ADAS-cog score" have HPD intervals that do not contain 0. We plotted the survival functions for male and female patients, where the values of other covariates are taken as the mean value of the covariates. Also the average patient whose the first/second allele in APOE4 is 3/4 or not, where the values of other covariates are taken as the mean value of the covariates. Also the average patient who have never married or not, where the values of other covariates

are taken as the mean value of the covariates; see Figure 5. It is noticed that the average female subjects tend to convert from MCI to AD more fastly than the average male subjects. The subjects who have type 2 of the first allele in APOE4 tend to convert from MCI to AD more fastly than the other subjects. The subjects with type 4 of the first allele in APOE4 are expected to convert from MCI to AD more fastly than the other subjects. The subjects who have married are more hazardous than the other subjects.

For Model 3, we only included the clinical characteristics, APOE genetic covariates, and ADAS-cog score as covariates. We applied BFLCRM to obtain the estimation results for the 12 covariates. Based on the 20,000 MCMC samples, "Gender", "Handedness", "Never married", "first allele in APOE4=3", "the first allele in APOE4=4, " "Second allele in APOE4=3", and "ADAS-cog score" have HPD intervals that do not contain 0. The 1st, 3rd, 7th, 9th and 11th fPCs have 95% HPD intervals that do not contain 0. We plotted the survival functions for male and female patients, where the values of other covariates are taken as the mean value of the covariates. Also the average patient whose the first/second allele in APOE4 is 3/4 or not, where the values of other covariates are taken as the mean value of the covariates. Also the average patient who have never married or not, where the values of other covariates are taken as the mean value of the covariates; see Figure 6. It is noticed that the average female subjects tend to convert from MCI to AD more fastly than the average male subjects. The subjects who have type 2 of the first allele in APOE4 tend to convert from MCI to AD more fastly than the other subjects. The subjects with type 3 of the first allele in APOE4 are expected to convert from MCI to AD more fastly than the other subjects. The subjects who have married are more hazardous than the other subjects.

Table 5 shows the summary measures of DIC and iAUC for the four models. The full model yields the DIC value of 639.68, which is smaller than those of Models 2 and 3, while larger than that of Model 1. The full model and Model 1 with the hippocampal surface data provide the better predictive performance than the others do. We estimated the iAUC by using a Monte Carlo cross-validation (MCCV) method [23]. The full data set was randomly split into training and test data, where the sample sizes of training and test data are 200 and 146, respectively. For each such split, we fitted the BFLCRM to the training data and then calculated iAUC based on the test data. This random split was repeated 100 times leading to 100 iAUC values. We calculated their sample mean and standard deviation as (0.80, 0.04), (0.77, 0.03), (0.74, 0.03), and (0.70, 0.03) for the full model, Model 1, Model 2, and Model 3, respectively. This may indicate that the functional

nature of the hippocampal surface data contributes to the explanation of the time to conversion in terms of prediction performance.

4. Simulation Studies. In this section, we conduct Monte Carlo simulations to evaluate the proposed BFLCRM at different censoring rates and sample sizes. Moreover, we will evaluate the predictability of our BFLCRM compared to the proportional hazards model without functional covariates.

4.1. *Setup.* We generated all simulated data sets according to model (2.1). We independently generated survival times T_i from an exponential distribution with parameter $\exp(\mathbf{x}_i^T\boldsymbol{\beta} + \int_0^1 \gamma(s)Z_i(s)ds)$. Thus, in this case, we have $h_0(s) = 1$. The $\boldsymbol{x}_i$ is a 4×1 vector and its corresponding elements were generated from $N(1.8, 0.20)$, $N(1.7, 0.30)$, $N(1.2, 0.25)$, and $N(-1, 0.25)$, respectively. We set the true $\boldsymbol{\beta}$ to be $(0.7, 0.2, -0.5, -1)$. The functional covariate $Z_i(s)$ was generated from model (2.3), in which the $\epsilon_i(s)$'s were independently simulated from a $N(0, 1)$ across s and the ξ_{ij}'s are independently generated from a $N(0, \psi_j)$ with $\psi_1 = 0.5$, $\psi_2 = 0.3$, $\psi_3 = 0.1$, $\psi_4 = 0.05$, $\psi_5 = 0.01$, $\psi_6 = 0.005$, and $\psi_k = 0$ for all $k \geq 7$. Moreover, we set the first six eigenfunctions as

$$\begin{aligned}
\phi_1(s) &= \sqrt{2}\sin((1-0.5)\pi s), \phi_2(s) = \sqrt{2}\sin((2-0.5)\pi s), \\
\phi_3(s) &= \sqrt{2}\sin((3-0.5)\pi s), \phi_4(s) = \sqrt{2}\sin((4-0.5)\pi s), \\
\phi_5(s) &= \sqrt{2}\sin((5-0.5)\pi s), \phi_6(t) = \sqrt{2}\sin((6-0.5)\pi s)
\end{aligned}$$

for $0 \leq s \leq 1$. We set $\gamma(s) = \phi_1(s) + 0.5\phi_2(s) + 0.25\phi_3(s)$ so that $\boldsymbol{\gamma} = (\gamma_1, \gamma_2, \gamma_3, \gamma_4, \cdots) = (1, 0.5, 0.25, 0, \cdots)$. The function values of $Z_i(s)$ were evaluated at 100 equally spaced grids in $[0, 1]$. Finally, the survival times were randomly right censored to achieve a desired censoring rate of 30% or 50%. We considered sample sizes of $n = 200$ and $n = 500$ for each censoring rate and simulated 100 data sets for each case.

4.2. *Simulation Results.* We used the piecewise constant hazard model for $H_0(s)$, in which we set $J = 100$ and subintervals $(s_{j-1}, s_j]$ to be of equal length. We set $(\alpha_{0j}, \alpha_{1j}) = (8.0, 10.0)$ for all j, $\boldsymbol{\Sigma}_0 = 0.25\text{diag}(1, \cdots, 1)$, and $\boldsymbol{\mu}_0 = (0.7, 0.2, -0.5, -1, 1, 0.5, 0.25, 0.0)^T$. We set $q_n = 4$ since the first 4 fPC scores explain 95% of the variation of the functional covariates. For each simulated data set, we ran the Gibbs sampler for 20,000 iterations with 5,000 burn-in iterations.

To examine the estimation and prediction performance of BFLCRM, we calculated mean squared errors (MSEs) and time-dependent integrated area

under the curve (iAUC)[23] based on 100 simulated data sets for each scenario. We let $\hat{\boldsymbol{\beta}}$ denote the posterior mean of $\boldsymbol{\beta}$. The MSE of $\hat{\boldsymbol{\beta}}$ is defined by $\text{MSE}_{\hat{\boldsymbol{\beta}}} = \sum_{j=1}^{p}(\hat{\beta}_j - \beta)^2$, whereas the MSE for $\gamma(\cdot)$ is defined by $\text{MSE}_{\hat{\gamma}} = \int_0^1 \{\hat{\gamma}(s) - \gamma(s)\}^2 ds$, where $\hat{\gamma}(s)$ denotes the posterior mean of γ at time s. A smaller MSE implies better estimation accuracy. A large value of iAUC implies a better predictive model. Particularly, the perfect predictive model achieves iAUC=1.

Table 6 presents the estimation results based on 100 simulated data sets for each scenario. The MSE values of both $\hat{\boldsymbol{\beta}}$ and $\hat{\gamma}(\cdot)$ are fairly small in all cases. The values of iAUC indicate reasonable predictive performance of our BFLCRM. The MSE value decreases as either the sample size gets larger or the censoring rate gets smaller.

To evaluate the predictive value of the functional covariate to the hazard function, we calculated iAUC for two nested models including a reduced model with solely scalar covariates in $\boldsymbol{x}_i$ and a full model with both $Z_i(\cdot)$ and $\boldsymbol{x}_i$. Table 7 presents the means and standard deviations of iAUC for the reduced and full models under each scenario. The iAUC value of the full model is generally larger than that of the reduced model in all scenarios. This may indicate that the use of functional covariates can improve predictability of the hazard function.

5. Discussion. The BFLCRM was developed to predict the time of conversion from MCI to AD, as well as to determine the optimal set of predictors at baseline that effect the time of conversion. We obtained estimation and prediction results for functional and scalar predictors. This study has examined a very large set of predictors for predicting the time of conversion from MCI to AD. We observed several important effects including, (i) gender, (ii) handedness, (iii) APOE status, and (v) surface morphology changes with the right and left hippocampi. These findings highlight the importance of including not only demographic and clinical information, but also high-dimensional imaging data, in statistical analyses of MCI-AD conversion, and are consistent with newly published clinical research criteria which incorporate the use of an array of biomarkers in research settings and clinical trials [1].

Several prior studies have highlighted the importance of hippocampal changes in the context of AD-related neurodegeneration and prediction of MCI-AD conversion [12]. These studies, however, commonly assess changes to hippocampal volume rather than surface morphology. The current analysis included both measures of volume and surface area, with the changes in surface morphology adding additional predictive value. As shown in Figure

X, the changes in surface area occur more prominently on the anterior portion of the long axis of the hippocampus. Functional MRI studies in healthy adults suggest that anterior portions of the hippocampus are critical for the mnemonic binding processes that are engaged in tasks of episodic (day-to-day) memory. Since episodic memory tasks, particularly those that require binding operations, are some of the earliest cognitive impairments observed in MCI-AD [2], the anterior surface changes identified in the current analysis may underlie these early memory changes and serve as an important predictor of time of conversion.

The analysis also showed that APOE status exerted important effects on the time of conversion. We included apolipoprotein E (APOE) genotype data in the model, as several prior studies have documented that the presence of the APOE e4 allele increases the risk of developing Alzheimer's disease. The results of our analysis showed that if the second allele of the APOE has type 3, MCI progression is less likely to occur.

We have demonstrated the utility of BFLCRM's as a valuable method for identifying optimal early markers of conversion to AD in patients with MCI. The early markers identified from our analysis could be used in case selection for various clinical trials for evaluating drug/therapeutic efficiency in slowing or modifying AD-related pathophysiology, when such drugs and therapeutic treatments are available.

There are some limitations to our analysis. Our findings survived internal cross validation but need replication in an independent community-based sample. We did not include measures of pathology (e.g. beta-amyloid) in our models since CSF and amyloid-PET were available only in a small subset of individuals in ADNI-1. However, a study of ADNI-2 subjects has shown a robust correlation between the APOE e4 allele and cortical amyloid burden [40], suggesting that APOE e4 may have served as a surrogate for cortical amyloid plaque load in our analysis.

We have developed a BFLCRM for the use of functional and scalar covariates to predict time-to-event outcomes. Several important methodological issues need to be addressed in future research. First, it is interesting to investigate the theoretical properties of our Bayesian procedure, including the support of the prior and truncation approximation bounds q_n. Second, it is interesting to develop a new Bayesian method to automatically determine the distribution of q_n. Third, it is interesting to incorporate high-dimensional scalar covariates (e.g., genetic markers in the whole genome) in FLCRM and develop its associated estimation and testing procedures. Developing such statistical methods poses many new challenges both computationally and theoretically.

Acknowledgements.

References.

[1] Albert, M. S., DeKosky, S. T., Dickson, D., Dubois, B., Feldman, H. H., Fox, N. C., Gamst, A., Holtzman, D. M., Jagust, W. J., Petersen, R. C., Snyder, P. J., Carrillo, M. C., Thies, B. and Phelps, C. H. (2011). The diagnosis of mild cognitive impairment due to Alzheimer's disease: Recommendations from the National Institute on Aging-Alzheimer's Association workgroups on diagnostic guidelines for Alzheimer's disease. *Alzheimer's & Dementia* **7** 270–279.

[2] Anderson, N. D., Ebert, P. L., Jennings, J. M., Grady, C. L., Cabeza, R. and Graham, S. J. (2008). Recollection-and familiarity-based memory in healthy aging and amnestic mild cognitive impairment. *Neuropsychology* **22** 177.

[3] Apostolova, L. G., Dinov, I. D., Dutton, R. A., Hayashi, K. M., Toga, A. W., Cummings, J. L. and Thompson, P. M. (2006). 3D comparison of hippocampal atrophy in amnestic mild cognitive impairment and Alzheimer's disease. *Brain* **129** 2867–2873.

[4] Biswas, A., Datta, S., Fine, J. P. and Segal, M. R. (2007). *Statistical advances in the biomedical sciences: clinical trials, epidemiology, survival analysis, and bioinformatics* **630**. John Wiley & Sons.

[5] Bryant, C., Giovanello, K. S., Ibrahim, J. G., Chang, J., Shen, D., Peterson, B. S., Zhu, H. and ADNI (2013). Mapping the Genetic Variation of Regional Brain Volumes as Explained by All Common SNPs from the ADNI Study. *PloS One* **8** e71723.

[6] Colom, R., Stein, J. L., Rajagopalan, P., Martínez, K., Hermel, D., Wang, Y., Álvarez-Linera, J., Burgaleta, M., Quiroga, M., Shih, P. C. and Thompson, P. M. (2013). Hippocampal structure and human cognition: Key role of spatial processing and evidence supporting the efficiency hypothesis in females. *Intelligence* **41** 129–140.

[7] Costafreda, S. G., Dinov, I. D., Tu, Z., Shi, Y., Liu, C. Y., Kloszewska, I., Mecocci, P., Soininen, H., Tsolaki, M., Vellas, B., Wahlund, L. O., Spenger, C., Toga, A. W., Lovestone, S. and Simmons, A. (2011). Automated hippocampal shape analysis predicts the onset of dementia in mild cognitive impairment. *Neuroimage* **56** 212–219.

[8] Cox, D. R. et al. (1972). Regression models and life tables. *J.R.Stat.Soc.B* **34** 187–220.

[9] Cui, Y., Liu, B., Luo, S., Zhen, X., Fan, M., Liu, T., Zhu, W., Park, M., Jiang, T., Jin, J. S. and ADNI (2011). Identification of conversion from mild cognitive impairment to Alzheimer's disease using multivariate predictors. *PloS One* **6** e21896.

[10] de la Torre, J. C. (2010). Alzheimer's disease is incurable but preventable. *Journal of Alzheimer's Disease* **20** 861–870.

[11] Desikan, R. S., Cabral, H. J., Fischl, B., Guttmann, C. R. G., Blacker, D., Hyman, B. T., Albert, M. S. and Killiany, R. J. (2009). Temporoparietal MR imaging measures of atrophy in subjects with mild cognitive impairment that predict subsequent diagnosis of Alzheimer disease. *American Journal of Neuroradiology* **30** 532–538.

[12] Dickerson, B. C., Wolk, D. A. and ADNI (2013). Biomarker-based prediction of progression in MCI: comparison of AD signature and hippocampal volume with spinal fluid amyloid-β and tau. *Frontiers in Aging Neuroscience* **5**.

[13] Dickerson, B. C., Goncharova, I., Sullivan, M. P., Forchetti, C., Wilson, R. S., Bennett, D. A., Beckett, L. A. and deToledo Morrell, L. (2001). MRI-derived entorhinal and hippocampal atrophy in incipient and very mild Alzheimer's disease. *Neurobiology of Aging* **22** 747–754.

[14] Fan, J. and Lv, J. (2010). A selective overview of variable selection in high dimensional feature space. *Statistica Sinica* **20** 101-148.

[15] Fan, Y., Batmanghelich, N., Clark, C. M. and Davatzikos, C. (2008). Spatial patterns of brain atrophy in MCI patients, identified via high-dimensional pattern classification, predict subsequent cognitive decline. *Neuroimage* **39** 1731–1743.

[16] Fennema-Notestine, C., Hagler, D. J., McEvoy, L. K., Fleisher, A. S., Wu, E. H., Karow, D. S. and Dale, A. M. (2009). Structural MRI biomarkers for preclinical and mild Alzheimer's disease. *Human Brain Mapping* **30** 3238–3253.

[17] Ferraty, F. and Vieu, P. (2006). *Nonparametric Functional Data Analysis: Methods, Theory, Applications and Implementation*. Springer, New York.

[18] Fleming, T. R. and Harrington, D. P. (2011). *Counting processes and survival analysis* **169**. John Wiley & Sons.

[19] Gauthier, S., Reisberg, B., Zaudig, M., Petersen, R. C., Ritchie, K., Broich, K., Belleville, S., Brodaty, H., Bennett, D., Chertkow, H., Cummings, J. L., de Leon, M., Feldman, H., Ganguli, M., Hampel, H., Scheltens, P., Tierney, M. C., Whitehouse, P. and Winblad, B. (2006). Mild cognitive impairment. *The Lancet* **367** 1262–1270.

[20] Gelman, A., Gilks, W. R. and Roberts, G. O. (1997). Weak convergence and optimal scaling of random walk Metropolis algorithms. *The Annals of Applied Probability* **7** 110–120.

[21] Grundman, M., Sencakova, D., Jack, C. R., Petersen, R. C., Kim, H. T., Schultz, A., Weiner, M. F., DeCarli, C., DeKosky, S. T., van Dyck, C., Thomas, R. G., Thal, L. J. and ADCS (2002). Brain MRI hippocampal volume and prediction of clinical status in a mild cognitive impairment trial. *Journal of Molecular Neuroscience* **19** 23–27.

[22] Hastings, W. K. (1970). Monte Carlo sampling methods using Markov chains and their applications. *Biometrika* **57** 97–109.

[23] Heagerty, P. J. and Zheng, Y. (2005). Survival model predictive accuracy and ROC curves. *Biometrics* **61** 92–105.

[24] Ibrahim, J. G., Chen, M. H. and Sinha, D. (2001). *Bayesian Survival Analysis*. New York: Springer-Verlag Inc.

[25] Ibrahim, J. G., Chen, M.-H. and Sinha, D. (2005). *Bayesian Survival Analysis*. Wiley Online Library.

[26] Ibrahim, J. G., Chen, M. H. and Kim, S. (2008). Bayesian variable selection for the Cox regression model with missing covariates. *Lifetime Data Analysis* **14** 496–520.

[27] Jack Jr, C. R., Knopman, D. S., Jagust, W. J., Shaw, L. M., Aisen, P. S., Weiner, M. W., Petersen, R. C. and Trojanowski, J. Q. (2010). Hypothetical model of dynamic biomarkers of the Alzheimer's pathological cascade. *The Lancet Neurology* **9** 119–128.

[28] James, G. (2002). Generalized linear models with functional predictors. *Journal of Royal Statistical Society B* **64** 411-432.

[29] Huang, J., Sun, T., Ying, Z., Y, Y. and Zhang, C. (2013). Oracle inequalities for the lasso in the Cox model. *Ann. Statist.* **41** 1142-1165.

[30] Kalbfleisch, J. D. (1978). Nonparametric Bayesian Analysis of Survival Time Data. *Journal of the Royal Statistical Society, Series B: Methodological* **40** 214–221.

[31] Kalbfleisch, J. D. and Prentice, R. L. (2002). *The Statistical Analysis of Failure*

Time Data. John Wiley & Sons.

[32] Kaye, J. A., Moore, M. M., Dame, A., Quinn, J., Camicioli, R., Howieson, D., Corbridge, E., Care, B., Nesbit, G. and Sexton, G. (2005). Asynchronous regional brain volume losses in presymptomatic to moderate AD. *Journal of Alzheimer's Disease* **8** 51–56.

[33] Li, J. and Ma, S. (2013). *Survival Analysis in Medicine and Genetics*. Chapman & Hall/CRC.

[34] Li, S., Okonkwo, O., Albert, M. and Wang, M. C. (2013). Variation in Variables that Predict Progression from MCI to AD Dementia over Duration of Follow-up. *American Journal of Alzheimer's Disease* **1** 12–28.

[35] Lorensen, W. E. and Cline, H. E. (1987). Marching cubes: A high resolution 3D surface construction algorithm. In *ACM Siggraph Computer Graphics* **21** 163–169. ACM.

[36] Luders, E., Thompson, P. M., Kurth, F., Hong, J. Y., Phillips, O. R., Wang, Y., Gutman, B. A., Chou, Y. Y., Narr, K. L. and Toga, A. W. (2013). Global and regional alterations of hippocampal anatomy in long-term meditation practitioners. *Human Brain Mapping* **34** 3369–3375.

[37] Metropolis, N., Rosenbluth, A. W., Rosenbluth, M. N., Teller, A. H. and Teller, E. (2004). Equation of state calculations by fast computing machines. *The Journal of Chemical Physics* **21** 1087–1092.

[38] Misra, C., Fan, Y. and Davatzikos, C. (2009). Baseline and longitudinal patterns of brain atrophy in MCI patients, and their use in prediction of short-term conversion to AD: results from ADNI. *Neuroimage* **44** 1415–1422.

[39] Monje, M., Thomason, M. E., Rigolo, L., Wang, Y., Waber, D. P., Sallan, S. E. and Golby, A. J. (2013). Functional and structural differences in the hippocampus associated with memory deficits in adult survivors of acute lymphoblastic leukemia. *Pediatric Blood & Cancer* **60** 293–300.

[40] Murphy, K. R., Landau, S. M., Choudhury, K. R., Hostage, C. A., Shpanskaya, K. S., Sair, H. I., Petrella, J. R., Wong, T. Z. and Doraiswamy, P. M. (2013). Mapping the effects of ApoE4, age and cognitive status on 18F-florbetapir PET measured regional cortical patterns of beta-amyloid density and growth. *Neuroimage* **78** 474–480.

[41] Patenaude, B., Smith, S. M., Kennedy, D. N. and Jenkinson, M. (2011). A Bayesian model of shape and appearance for subcortical brain segmentation. *Neuroimage* **56** 907–922.

[42] Pennanen, C., Kivipelto, M., Tuomainen, S., Hartikainen, P., Hänninen, T., Laakso, M. P., Hallikainen, M., Vanhanen, M., Nissinen, A., Helkala, E. L., Vainio, P., Vanninen, R., Partanen, K. and Soininen, H. (2004). Hippocampus and entorhinal cortex in mild cognitive impairment and early AD. *Neurobiology of Aging* **25** 303–310.

[43] Perri, R., Serra, L., Carlesimo, G. A. and Caltagirone, C. (2007). Amnestic mild cognitive impairment: difference of memory profile in subjects who converted or did not convert to Alzheimer's disease. *Neuropsychology* **21** 549.

[44] Petersen, R. C., Thomas, R. G., Grundman, M., Bennett, D., Doody, R., Ferris, S., Galasko, D., Jin, S., Kaye, J., Levey, A., Pfeiffer, E., Sano, M., van Dyck, C. H., Thal, L. J. and ADCSG (2005). Vitamin E and donepezil for the treatment of mild cognitive impairment. *New England Journal of Medicine* **352** 2379–2388.

[45] Pizer, S. M., Fritsch, D. S., Yushkevich, P. A., Johnson, V. E. and Chaney, E. L. (1999). Segmentation, registration, and measurement of shape vari-

ation via image object shape. *IEEE Transactions on Medical Imaging* **18** 851–865.

[46] Prestia, A., Caroli, A., van der Flier, W. M., Ossenkoppele, R., Van Berckel, B., Barkhof, F., Teunissen, C. E., Wall, A. E., Carter, S. F., Schöll, M., Choo, I. H., Nordberg, A., Scheltens, P. and Frisoni, G. B. (2013). Prediction of dementia in MCI patients based on core diagnostic markers for Alzheimer disease. *Neurology* **80** 1048–1056.

[47] Ramsay, J. O. and Silverman, B. W. (2005). *Functional Data Analysis*. Springer-Verlag, New York.

[48] Reiss, P. T. and Ogden, R. T. (2010). Functional generalized linear models with images as predictors. *Biometrics* **66** 61-69.

[49] Risacher, S. L., Saykin, A. J., Wes, J. D., Shen, L., Firpi, H. A. and McDonald, B. C. (2009). Baseline MRI predictors of conversion from MCI to probable AD in the ADNI cohort. *Current Alzheimer Research* **6** 347–361.

[50] Rosen, W. G., Mohs, R. C. and Davis, K. L. (1984). A new rating scale for Alzheimer's disease. *The American Journal of Psychiatry* **141** 1356-1364.

[51] Shaw, L. M., Vanderstichele, H., Knapik-Czajka, M., Clark, C. M., Aisen, P. S., Petersen, R. C., Blennow, K., Soares, H., Simon, A., Lewczuk, P., Dean, R., Siemers, E., Potter, W., Lee, V. M., Trojanowski, J. Q. and ADNI (2009). Cerebrospinal fluid biomarker signature in Alzheimer's disease neuroimaging initiative subjects. *Annals of Neurology* **65** 403–413.

[52] Shi, J., Thompson, P. M., Gutman, B. and Wang, Y. (2013a). Surface fluid registration of conformal representation: Application to detect disease burden and genetic influence on hippocampus. *NeuroImage* **78** 111–134.

[53] Shi, J., Wang, Y., Ceschin, R., An, X., Lao, Y., Vanderbilt, D., Nelson, M. D., Thompson, P. M., Panigrahy, A. and Leporé, N. (2013b). A multivariate surface-based analysis of the putamen in premature newborns: Regional differences within the ventral striatum. *PloS One* **8** e66736.

[54] Sinha, D., Ibrahim, J. G. and Chen, M. H. (2003). A Bayesian Justification of Cox's Partial Likelihood. *Biometrika* **90** 629-641.

[55] Tabert, M. H., Manly, J. J., Liu, X., Pelton, G. H., Rosenblum, S., Jacobs, M., Zamora, D., Goodkind, M., Bell, K., Stern, Y. and Devanand, D. P. (2006). Neuropsychological prediction of conversion to Alzheimer disease in patients with mild cognitive impairment. *Archives of General Psychiatry* **63** 916–924.

[56] Tibshirani, R. (1996). Regression shrinkage and selection via the lasso. *J. Roy. Statist. Soc. Ser. B* **58** 267-288. MR1379242 (96j:62134)

[57] Vemuri, P., Gunter, J. L., Senjem, M. L., Whitwell, J. L., Kantarci, K., Knopman, D. S., Boeve, B. F., Petersen, R. C. and Jack Jr, C. R. (2008). Alzheimer's disease diagnosis in individual subjects using structural MR images: validation studies. *Neuroimage* **39** 1186–1197.

[58] Wang, Y., Zhang, J., Gutman, B., Chan, T. F., Becker, J. T., Aizenstein, H. J., Lopez, O. L., Tamburo, R. J., Toga, A. W. and Thompson, P. M. (2010). Multivariate tensor-based morphometry on surfaces: application to mapping ventricular abnormalities in HIV/AIDS. *NeuroImage* **49** 2141–2157.

[59] Yao, F., Muller, H. G. and Wang, J. L. (2005). Functional linear regression analysis for longitudinal data. *The Annals of Statistics* **33** 2873–2903.

[60] Young, J., Modat, M., Cardoso, M. J., Mendelson, A., Cash, D. and Ourselin, S. (2013). Accurate multimodal probabilistic prediction of conversion to Alzheimer's disease in patients with mild cognitive impairment. *NeuroImage: Clinical* **2** 735–745.

[61] Zhang, D., Shen, D. and ADNI (2012). Predicting future clinical changes of MCI patients using longitudinal and multimodal biomarkers. *PloS One* **7** e33182.

TABLE 1

ADNI data analysis results for the full model: the posterior quantities of 19 regression coefficients β_ks, that correspond to $\boldsymbol{x}_i$ =(Gender, Handedness, Married, Widowed, Divorced, Length of Education, Retirement, Age, the First Allele in APOE4=3, the First Allele in APOE4=4, the Second Allele in APOE4=3, ADAS-cog Score, Right hippocampal formation, Left hippocampal formation, Left amygdala, Right amygdala, posterior limb of internal capsule, and Left thalamus). Mean denotes 'posterior mean', SD denotes 'posterior standard deviation', and lower and upper, respectively, represent the lower and upper limits of a 95% highest posterior density interval.

	β_1	β_2	β_3	β_4	β_5	β_6	β_7	β_8	β_9
Mean	0.3671	0.2259	0.1285	0.1294	0.8298	-0.0387	0.1409	-0.0260	0.1031
SD	0.0849	0.0935	0.0942	0.0948	0.0994	0.0242	0.0872	0.0124	0.0169
lower	0.1990	0.0320	-0.0480	-0.0690	0.6450	-0.0820	-0.0270	-0.0510	0.0680
upper	0.5320	0.3970	0.3240	0.2940	1.0230	0.0100	0.3110	0.0030	0.1340

	β_{10}	β_{11}	β_{12}	β_{13}	β_{14}	β_{15}	β_{16}	β_{17}	β_{18}	β_{19}
Mean	0.4673	0.3684	-0.3787	0.0005	0.0003	-0.0004	-0.0002	0.0010	-0.0008	0.0001
SD	0.0898	0.0873	0.0835	0.0005	0.0005	0.0005	0.0004	0.0007	0.0005	0.0003
lower	0.3020	0.1940	-0.5430	0.0000	0.0000	-0.0010	-0.0010	0.0000	-0.0010	0.0000
upper	0.6520	0.5310	-0.2280	0.0010	0.0010	0.0000	0.0000	0.0020	0.0000	0.0010

TABLE 2

ADNI data analysis results for Model 1: the posterior quantities of 19 regression coefficients β_ks, that correspond to $\boldsymbol{x}_i$ =(Gender, Handedness, Married, Widowed, Divorced, Length of Education, Retirement, Age, the First Allele in APOE4=3, the First Allele in APOE4=4, the Second Allele in APOE4=3, and ADAS-cog Score). Mean denotes 'posterior mean', SD denotes 'posterior standard deviation', and lower and upper, respectively, represent the lower and upper limits of a 95% highest posterior density interval.

	β_1	β_2	β_3	β_4	β_5	β_6	β_7	β_8	β_9	β_{10}	β_{11}	β_{12}
Mean	0.394	0.252	0.141	0.050	0.538	-0.032	0.229	-0.019	0.428	0.299	-0.418	0.109
SD	0.082	0.095	0.088	0.095	0.102	0.024	0.091	0.012	0.084	0.094	0.086	0.018
lower	0.234	0.065	-0.033	-0.131	0.333	-0.077	0.057	-0.043	0.267	0.114	-0.588	0.072
upper	0.545	0.440	0.304	0.233	0.725	0.015	0.410	0.002	0.592	0.472	-0.261	0.142

EUNJEE LEE, HONGTU ZHU,
DEHAN KONG, KELLY SULLIVAN GIOVANELLO, JOSEPH G IBRAHIM
DEPARTMENT OF BIOSTATISTICS, PSYCHOLOGY AND
BIOMEDICAL RESEARCH IMAGING CENTER,
UNIVERSITY OF NORTH CAROLINA AT CHAPEL HILL,
CHAPEL HILL, NC 27599, USA
E-MAIL: eunjee2@live.unc.edu
E-MAIL: hzhu@bios.unc.edu
E-MAIL: kongd@live.unc.edu
E-MAIL: kgio@email.unc.edu
E-MAIL: ibrahim@bios.unc.edu

YALIN WANG
SCHOOL OF COMPUTING, INFORMATICS, AND
DECISION SYSTEMS ENGINEERING
ARIZONA STATE UNIVERSITY
TEMPE, AZ 85287-8809
E-MAIL: ylwang@asu.edu

TABLE 3

ADNI data analysis results for the full model: the posterior quantities of 19 regression coefficients β_ks, that correspond to $\boldsymbol{x}_i$ =(Gender, Handedness, Married, Widowed, Divorced, Length of Education, Retirement, Age, the First Allele in APOE4=3, the First Allele in APOE4=4, the Second Allele in APOE4=3, ADAS-cog Score, Right hippocampal formation, Left hippocampal formation, Left amygdala, Right amygdala, posterior limb of internal capsule, and Left thalamus). Mean denotes 'posterior mean', SD denotes 'posterior standard deviation', and lower and upper, respectively, represent the lower and upper limits of a 95% highest posterior density interval.

	β_1	β_2	β_3	β_4	β_5	β_6	β_7	β_8	β_9
Mean	0.284	0.107	0.008	0.200	1.018	-0.030	0.055	-0.022	0.097
SD	0.087	0.094	0.087	0.092	0.097	0.022	0.092	0.012	0.019
lower	0.115	-0.077	-0.162	0.008	0.835	-0.074	-0.125	-0.045	0.059
upper	0.452	0.282	0.180	0.371	1.204	0.012	0.235	0.001	0.132

	β_{10}	β_{11}	β_{12}	β_{13}	β_{14}	β_{15}	β_{16}	β_{17}	β_{18}	β_{19}
Mean	0.583	0.538	-0.397	0.0006	0.0000	-0.0007	-0.0004	0.0011	-0.0006	0.0002
SD	0.091	0.090	0.089	0.0005	0.0002	0.0005	0.0005	0.0007	0.0005	0.0004
lower	0.387	0.367	-0.559	0.0000	0.0000	-0.0010	-0.0010	0.0000	-0.0010	0.0000
upper	0.744	0.710	-0.212	0.0010	0.0000	0.0000	0.0000	0.0020	0.0000	0.0010

TABLE 4

ADNI data analysis results for Model 1: the posterior quantities of 19 regression coefficients β_ks, that correspond to $\boldsymbol{x}_i$ =(Gender, Handedness, Married, Widowed, Divorced, Length of Education, Retirement, Age, the First Allele in APOE4=3, the First Allele in APOE4=4, the Second Allele in APOE4=3, and ADAS-cog Score). Mean denotes 'posterior mean', SD denotes 'posterior standard deviation', and lower and upper, respectively, represent the lower and upper limits of a 95% highest posterior density interval.

	β_1	β_2	β_3	β_4	β_5	β_6	β_7	β_8	β_9	β_{10}	β_{11}	β_{12}
Mean	0.329	0.296	0.031	0.017	0.748	-0.006	0.100	0.007	0.720	0.711	-0.509	0.116
SD	0.083	0.094	0.089	0.095	0.097	0.023	0.086	0.010	0.089	0.091	0.082	0.016
lower	0.170	0.110	-0.138	-0.171	0.557	-0.052	-0.064	-0.014	0.551	0.538	-0.669	0.085
upper	0.491	0.475	0.204	0.198	0.935	0.037	0.270	0.026	0.896	0.891	-0.353	0.148

TABLE 5

ADNI data analysis results: DIC for each model and the mean iAUC and the corresponding standard error in the parenthesis calculated from the Monte Carlo cross-validation (MCCV).

	Full model	Model 1	Model 2	Model 3
DIC	639.680	638.08142	641.46183	663.7984
iAUC	0.796 (0.039)	0.766 (0.034)	0.744 (0.034)	0.695 (0.031)

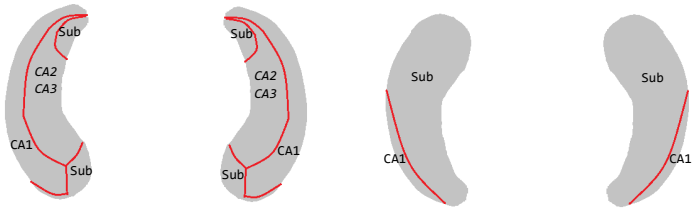

(a) Hippocampal subfields

(b) Top (c) Bottom (d) Color bar

Fig 1: ADNI data analysis results for the full model: panels (a) is hippocampal subfields mapped onto a representative hippocampal surface [3]. Panels (b) and (c), respectively, show the top and bottom views of the estimated coefficient function associated with the hippocampal surface data color-coded by the colorbar in panel (d). The subfields of CA1, CA2, CA3, and subicular on the hippocampus have negative effects on the hazard function.

TABLE 6

Simulation results under different censoring rates and sample sizes: the mean squared errors (MSE) of $\hat{\boldsymbol{\beta}}$ and $\hat{\gamma}$ and the estimated integrated area under the curve (iAUC), and their standard deviations in parentheses calculated from the 100 simulated data sets. The Gibbs sampler was run for 20,000 iterations with 5,000 burn-in iterations for each simulated data set.

n	censoring rate	$\text{MSE}_{\hat{\boldsymbol{\beta}}}$	$\text{MSE}_{\hat{\gamma}}$	iAUC
200	0.3	0.014 (0.0018)	0.041 (0.0046)	0.810 (0.0024)
500	0.3	0.002 (0.0012)	0.021 (0.0023)	0.814 (0.0022)
200	0.5	0.041 (0.0035)	0.197 (0.0072)	0.807 (0.0028)
500	0.5	0.020 (0.0019)	0.097 (0.0055)	0.809 (0.0024)

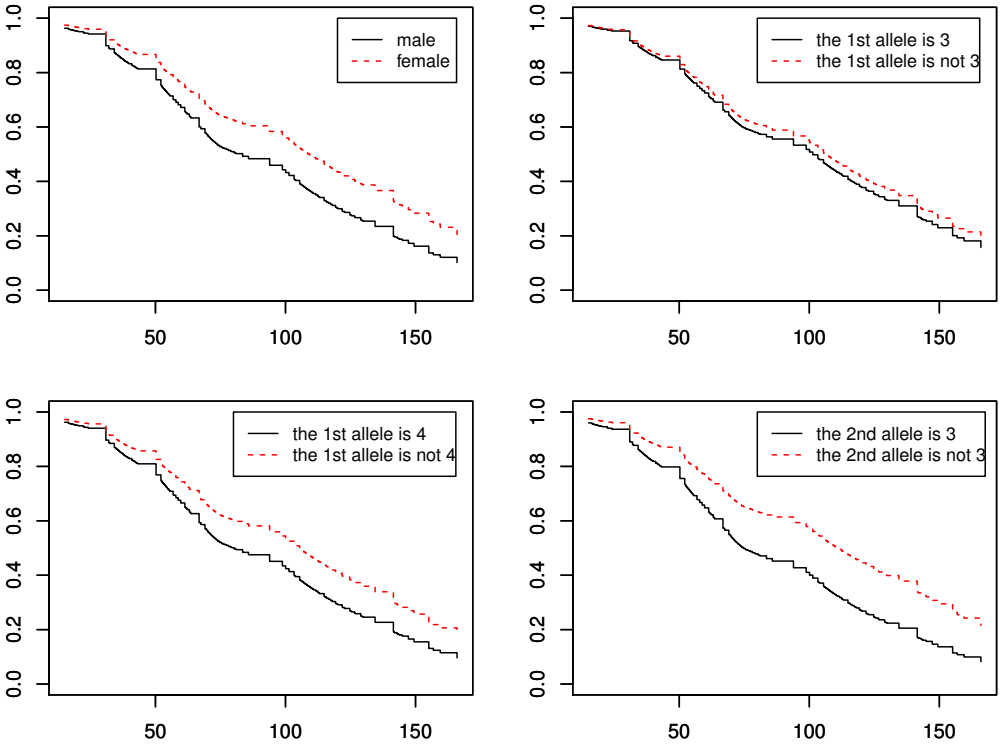

Fig 2: ADNI data analysis results for the full model: The top left panel shows the estimated survival function for average male and female subjects. The top right panel shows the estimated survival function for three types of the first allele in APOE4. The bottom left panel shows the estimated survival function for two types of the second allele in APOE4. The bottom right panel shows the estimated survival function for average "Never married" and "Have married" subjects.

(a) Top (b) Bottom (c) Color bar

Fig 3: ADNI data analysis results for Model 1: panels (a) and (b), respectively, show the top and bottom views of the estimated coefficient function associated with the hippocampal surface data color-coded by the colorbar in panel (c). The subfields of CA1, CA2, CA3, and subicular on the hippocampus have negative effects on the hazard function.

TABLE 7

Simulation results: the mean iAUC and the corresponding standard error in the parenthesis calculated from the 100 simulated data sets for each scenario. The Gibbs sampler was run for 20,000 iterations with 5,000 burn-in iterations for each simulated data set.

censoring rate	0.3		0.5	
n	200	500	200	500
reduced model	0.798 (0.005)	0.797 (0.004)	0.778 (0.004)	0.782 (0.004)
full model	0.81 (0.006)	0.814 (0.006)	0.807 (0.005)	0.809 (0.004)

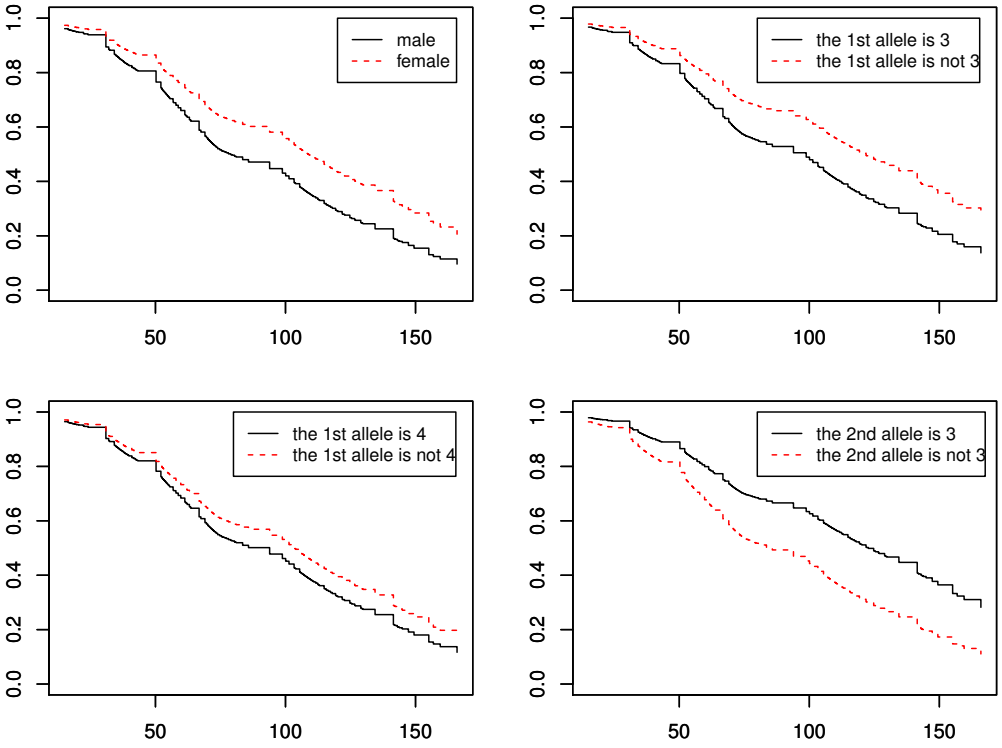

Fig 4: ADNI data analysis results for Model 1: The top left panel shows the estimated survival function for average male and female subjects. The top right panel shows the estimated survival function for three types of the first allele in APOE4. The bottom left panel shows the estimated survival function for two types of the second allele in APOE4. The bottom right panel shows the estimated survival function for average "Never married" and "Have married" subjects.

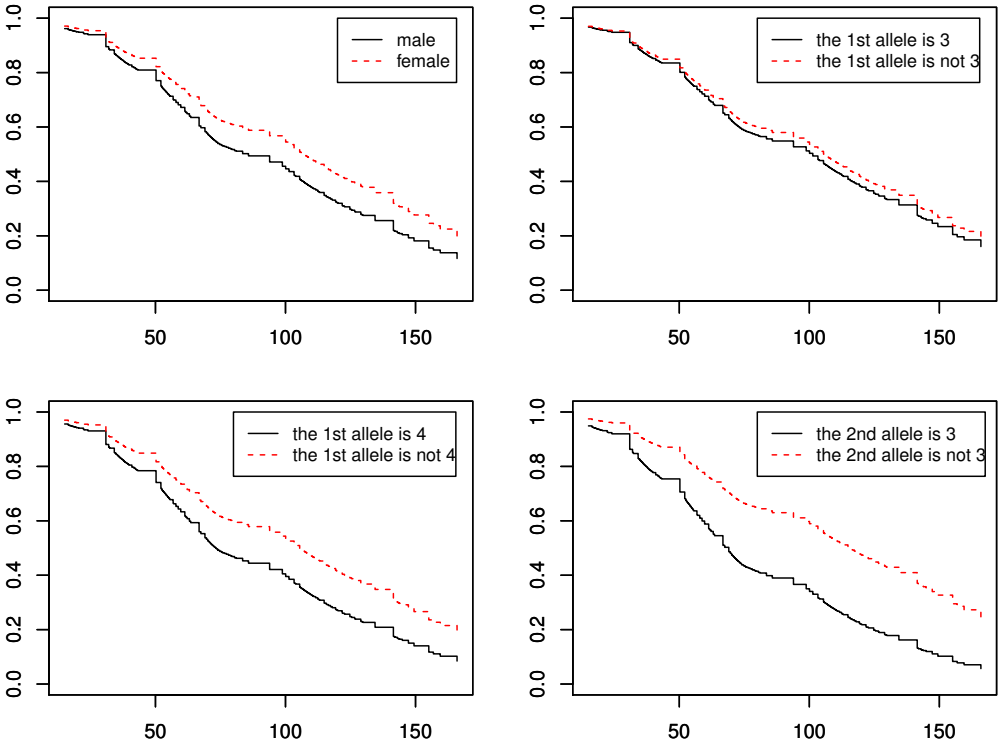

Fig 5: ADNI data analysis results for Model 2: The top left panel shows the estimated survival function for average male and female subjects. The top right panel shows the estimated survival function for three types of the first allele in APOE4. The bottom left panel shows the estimated survival function for two types of the second allele in APOE4. "The bottom right panel shows the estimated survival function for average "Never married" and "Have married" subjects.

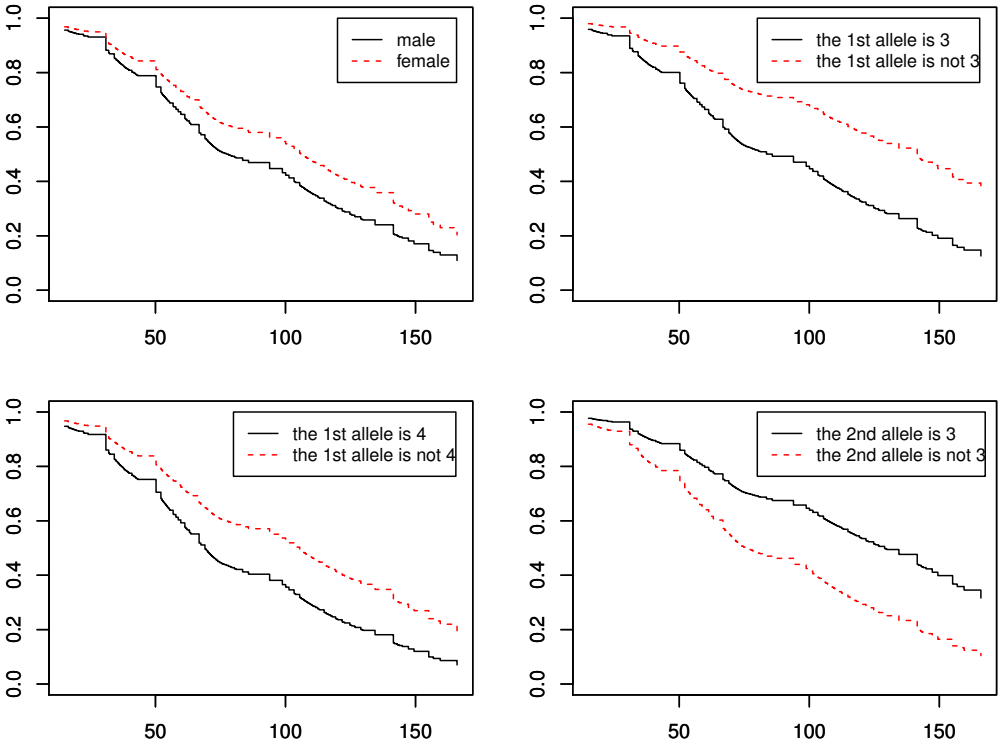

Fig 6: ADNI data analysis results for Model 3: The top left panel shows the estimated survival function for average male and female subjects. The top right panel shows the estimated survival function for three types of the first allele in APOE4. The bottom left panel shows the estimated survival function for two types of the second allele in APOE4. The bottom right panel shows the estimated survival function for average "Never married" and "Have married" subjects.

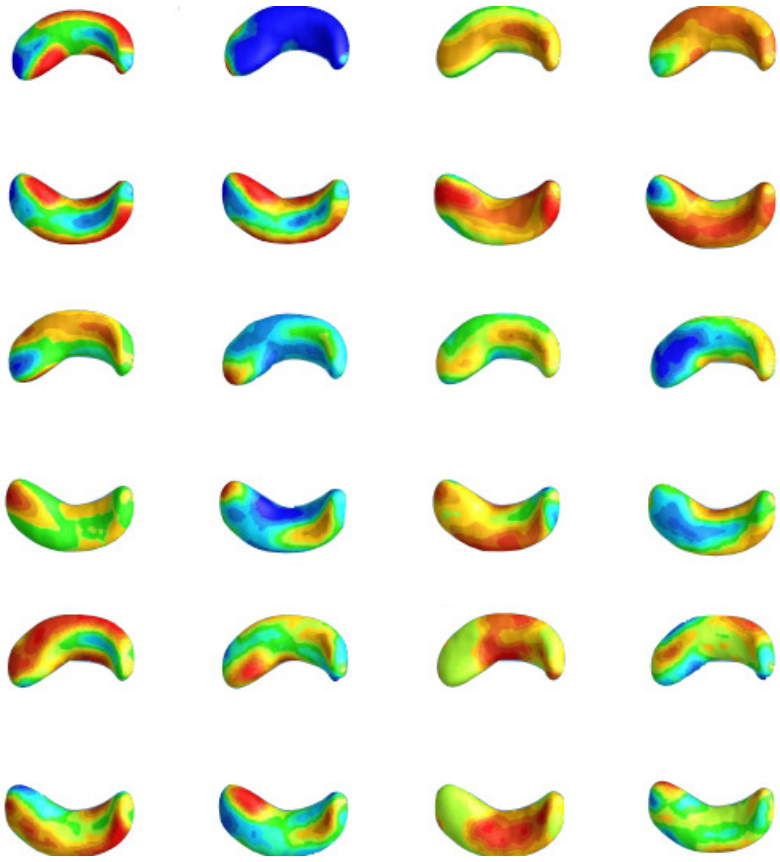

Fig 7: ADNI data analysis results: the first 12 largest estimated eigenfunctions projected on the hippocampal surface.